Degradation of Tris(1-chloro-2-propanyl) Phosphate by the Synergistic Effect of Persulfate and Zero-valent Iron During a Mechanochemical Process

Weichuan Qiao (hgqwc@njfu.edu.cn)
Nanjing Forestry University https://orcid.org/0000-0001-9721-9364
Qiwen Yang
Nanjing Forestry University
Yi Qian
Nanjing Forestry University
Ziyan Zhang
Nanjing Forestry University

Research Article

Keywords: Tris(1-chloro-2-propanyl) phosphate, Persulfate, Mechanochemical, Zero-valent iron, Dechlorination, Degradation

Posted Date: August 13th, 2021

DOI: https://doi.org/10.21203/rs.3.rs-576669/v1

Version of Record: A version of this preprint was published at Environmental Science and Pollution Research on January 17th, 2022. See the published version at https://doi.org/10.1007/s11356-022-18665-6.

Degradation of tris(1-chloro-2-propanyl) phosphate by the synergistic effect of persulfate and zero-valent iron during a mechanochemical process

Weichuan Qiao[a,b,*], Qiwen Yang[a], Yi Qian[a], Ziyan Zhang[a]

[a] Department of Environmental Engineering, College of Biology and the Environment, Nanjing Forestry University, Nanjing 210037, China

[b] Nanjing Yi Wei Environmental Protection Technology Co., Ltd., Nanjing 210048, China

* Corresponding authors. E-mail address: hgqwc@njfu.edu.cn (W. Qiao)

Abstract

This study revealed a dual pathway for the degradation of tris (1-chloro-2-propanyl) phosphate (TCPP) by zero-valent iron (ZVI) and persulfate as co-milling agents in a mechanochemical (MC) process. Persulfate was activated with ZVI to degrade TCPP in a planetary ball mill. After milling for 2 h, 96.5% of the TCPP was degraded with the release of 63.16, 50.39 and 42.01% of the Cl^-, SO_4^{2-} and PO_4^{3-}, respectively. In the first degradation pathway, persulfate was activated with ZVI to produce hydroxyl (·OH) radicals and ZVI is oxidized to Fe(Ⅱ) and Fe(Ⅲ). A substitution reaction occurred as a result of the attack of ·OH on the P–O–C bonds, leading to the successive breakage of the three P–O–C bonds in TCPP to produce PO_4^{3-}. In the second pathway, a C–Cl bond in part of the TCPP molecule was oxidized by $SO_4{\cdot}^-$ to carbonyl and carboxyl groups. The P–O–C bonds continued to react with ·OH to produce PO_4^{3-}. Finally, the intermediate organochloride products were further reductively dechlorinated by ZVI. However, the synergistic effect of the oxidation (·OH and $SO_4{\cdot}^-$) and the reduction reaction (ZVI) did not completely degrade TCPP to CO_2, resulting in a low mineralization rate (35.87%). Moreover, the intermediate products still showed the toxicities in LD_{50} and developmental toxicant. In addition, the method was applied for the degradation of TCPP in soil, and high degradations (>83.83%) were achieved in different types of soils.

Keywords: Tris(1-chloro-2-propanyl) phosphate; Persulfate; Mechanochemical; Zero-

valent iron; Dechlorination; Degradation

Speciality: Phosphorus flame retardants; Advanced oxidation process; Ball milling

1. Introduction

Brominated flame retardants (BFRs) have been banned in Europe on the grounds of their toxicity (Veen & Boer, 2012). They have been replaced by phosphorus flame retardants (PFRs), which are used to prevent the spread of flames after combustion and to delay ignition. PFRs are widely used in the textile and electronics industries, in transportation and in home improvement materials (Veen & Boer, 2012). However, PFRs can be released to the environment via volatilization, product wear and leakage during production and use. Although PFRs are not listed as persistent organic pollutants (POPs), they are long-lived in the environment (Quintana et al., 2008). As a typical PFRs, tris(1-chloro-2-propanyl) phosphate (TCPP) has a potential toxicity which is similar with BFRs (Björklund et al., 2004). Thus, TCPP should be removed from the environment as a matter of urgency.

TCPP has been detected in water, air, soil and organisms (Un-Jung et al., 2017, Wang et al., 2017). The levels of TCPP in surface water range from 0.05 μg/L to 10 μg/L, and those in river sediments were up to 165 μg/kg dw. Previous reports have shown that TCPP is both carcinogenic and teratogenic and accumulates in the liver and kidneys, resulting in a decrease of the number of cells and a change in neurotransmitters (Hoffman et al., 2014). Mechanochemical (MC) destruction is an effective and environmentally friendly method of removing chlorinated organic pollutants (Yan et al., 2017). Unlike photocatalytic and microbial degradation (Jurgens et al., 2014, Ruan et al., 2013), MC degradation is inexpensive, rapid, efficient, produces harmless

degradation products (Cagnetta et al., 2016) and has been used for the degradation of persistent organic pollutants (Veen & Boer, 2012). However, the MC degradation of TCPP has not been reported previously.

In the MC process, chemical reagents are activated by the high mechanical energy in a ball-milling reactor and the bonds in the target pollutants are destroyed as a result of the change in the morphology and crystal structure of the pollutant (Dubinskaya, 2010). TCPP contains P–O–C and C–Cl bonds, which both have important roles in maintaining the stability and toxicity of POPs. However, the use of MC processes to simultaneously degrade pollutants containing both phosphorus and chlorine has not been reported previously. We suggest that the mechanisms of the MC degradation of TCPP are different from those of other POPs.

Metals and metal oxides have been used as co-milling reagents to enhance the efficiency of the MC process in ball-milling (Fan et al., 2018, Yan et al., 2017). As a strong oxide, persulfate is widely used in the degradation of organic matter. It can be activated by heat, alkalis, ultraviolet light, microwave irradiation and transition metals to form highly active sulfate radicals ($SO_4\cdot^-$) that react with organic molecules (Oh et al., 2009, Wei et al., 2016). Also, persulfate can be activated by MC process with NaOH or CaO to degrade organic pollutants (Fan et al., 2020, Yan et al., 2015). Previous studies have shown that zero-valent iron (ZVI), Fe^{2+} and Fe^{3+}can activate persulfate (Oh et al., 2009, Wei et al., 2016, Yan et al., 2017). Under the action of free radicals, the C–Cl bonds of organic pollutants are broken and organic substances gradually

become inorganic substances, eventually resulting in mineralization (Cagnetta et al., 2017). In the MC process, zero-valent metals or metal oxides have been used as co-milling reagents with persulfate to enhance the MC degradation of pollutants (Liu et al., 2016a, Wang et al., 2019). However, the degradation of chlorinated organic compounds via a MC process with both ZVI and persulfate as co-milling agents has not yet been reported, and the degradation mechanisms remain unclear. Especially, the synergistic effect of the reduction of ZVI and the oxidation reaction of $SO_4\cdot^-$ in MC process on pollutants degradation need to be further explored.

ZVI and persulfate were used as co-milling reagents to remove TCPP in a planetary ball mill. The objectives of this study were to reveal the mechanism by which a persulfate+Fe+mechanochemical (PS+Fe^0+MC) process can use activated persulfate to degrade TCPP. The degradation intermediates and final products of TCPP were to be identified. The aim was to determine the pathway for the degradation of TCPP by this MC method to develop a new method for the remediation of chlorinated organic compounds.

2. Materials and methods

2.1. Materials

The TCPP ($C_9H_{18}Cl_3PO_4$, ≥98% purity) was purchased from Shanghai Rhawn Technology Development (Shanghai, China). This product contains two isomers (Fig. S1 and Table S1): tri(chloro-isopropyl) phosphate and *bis*-(1-chloro-2-propyl) (3-chloro-1-propyl) phosphate, referred to here as TCPP 1 and TCPP 2 , respectively. Iron

powder (100 mesh) was obtained from Shanghai Macklin Biochemical (Shanghai, China). Potassium persulphate ($K_2S_2O_8$, ≥98% purity) and the solvents (methanol, ethyl acetate and absolute ethanol) used in the gas chromatography–mass spectrometry (GC–MS) analyses were all purchased from Sinopharm Chemical Reagent (Shanghai, China). Ethyl acetate was purchased from Sinopharm Chemical Reagent Co., Ltd., Shanghai, China. All other chemical reagents and organic solvents were of analytical-reagent grade.

Three soils were collected from Liaoning (red soil), Jiangsu (yellow soil) and Heilongjiang (black soil) in China, respectively. All the soils were air-dried for one week ground and passed through a 1-mm mesh screen. The selected soil was stored at 4 ℃ and used as natural soil.

2.2. Ball-milling experiment

The MC experiment was performed in a planetary ball mill (QM-1SP2, Nanjing University Instrument Corp., Nanjing, China). Different ratios of iron powder and persulfate were mixed with the TCPP as co-milling reagents to give different weight ratios. The Fe^0+persulfate+TCPP mixture weighed 5 g. 150g of stainless-steel balls with diameters of 5 and 8 mm were placed into two 500-mL stainless-steel pots. The planetary ball mill was operated at a speed of 300~500 rev min^{-1} and the direction of rotation changed automatically every 45 min, including a 15 min pause for cooling. All

the experiments were performed in triplicate. The values of the mean and standard deviation were calculated by SPSS 19.0 software.

2.3. MC degradation of TCPP in soil

4.5g of different types of soil with 200 mg/kg of TCPP, 1g of iron powder and 0.25g of persulfate was mixed and added into the ball milling tank with 30:1 of the ball material mass ratio (BMR). The planetary ball mill was operated at a speed of 400 rpm, and the rotation direction changed automatically every 45 min, including 15min pause cooling time. All experiments were performed in triplicate.

2.4. Determination of TCPP and the degradation product

To determine the concentration of TCPP and the degradation product, 0.05 g of each ground sample was extracted with 10 mL of ethyl acetate and concentrated to 1 mL in a rotary evaporator (Rotavapor R-200, Buchi, Flawil, Switzerland) (Liu et al., 2016b). The concentration of TCPP was determined by GC/MS/MS using an Agilent 7000B system equipped with a DB-1 column (30m×0.25mm×1.00μm) (Agilent Technologies Inc., USA). The column temperature was increased from 60 to 280℃ (held for 1 min) at 15℃ min^{-1} and the residence time of the solvent was 5 min. The carrier gas was 99.999% He. The mass spectrometer transmission line and the ion source temperature were both 250℃ and the mass scan range was 30～400.

The degradation products of TCPP were qualitatively determined by liquid chromatography–quadrupole time-of-flight mass spectrometry (LC–QTOF-MS) using

a Shimadzu LC 30A + AB Sciex Triple TOF 5600^+ system equipped with a Agilent ZORBAX SB-C18 column (100 mm × 2.1 mm × 3.5 μm). The column temperature was 40℃. The measurements were performed in the positive ion mode by gradient elution using water (containing 0.1% formic acid) and acetonitrile at a flow-rate of 0.3 mL/min. The mass scan range was 50~1000 (Yu et al., 2019).

2.5. Determination of Cl^-, SO_4^{2-} and PO_4^{3-}

After MC treatment, 0.01g of each sample was dissolved in 20 mL of Milli-Q water. The mixture was stirred with a magnetic stirrer for 20 min at 80℃ and then treated ultrasonically for 30 min before filtration through a 0.47 μm fiber filter (Zhang et al., 2011). Cl^-, SO_4^{2-} and PO_4^{3-} were determined in the collected filtrate using an ICS900 ion chromatography system (Dionex, USA) equipped with a IonPac AG23 Guard Column (4 × 50 mm). The column temperature was 25℃ with a flow-rate of 1 mL/min and current intensity of the anion was 35 mA. The change in ion concentration was calculated by the release rate:

$$\text{Release rate} = (C_t - C_0)/C_0$$

where C_t is the concentration of the ion at t (min) and C_0 is the concentration of the ion at 0 min.

2.6. Instrumental analysis

Different methods of analysis were used to characterize the ball-milling samples collected at different times in the ball-milling experiment to clarify the mechanism of TCPP degradation by the MC process. Raman spectra were recorded using a DXR532

microscopic confocal Raman spectrometer (Thermo Fisher Scientific, USA) with an Ar laser beam at 514.5 nm and a scan range of 400~2500 cm^{-1} (Liu et al., 2016b). The infrared spectra were measured with the KBr disk method using a Thermo Fisher Scientific Nicolet IS5 Fourier transform infrared (FTIR) spectrometer in the range 400~4000 cm^{-1} (Dong et al., 2019).

The crystal structure of the ball-milling sample was analyzed with an Ultima IV X-ray diffraction (XRD) spectrometer (Rigaku Electric Co., Ltd, Japan) in the range 2θ = 10~90° at a step size of 0.02° (Sui et al., 2017). The elemental distribution and micro-morphology of the ball-milling samples were analyzed by field-emission scanning electron microscopy using an FEI Quanta 400 FEG (Quanta, USA). The changes in the valence states of the elements in the ball-milling samples were analyzed by X-ray photoelectron spectrometry (XPS) using a ESCALAB 250Xi spectrometer (Thermo Fisher Scientific, USA) and the binding energy scale was calibrated by the C1s peak at 284.8 eV (Dong et al., 2019). The active species and free radical were determined by an electron spin resonance (ESR) using Bruker ESR A320 (Germany).

2.7. Statistical analysis

All the data were mean ± standard deviation values from three different experiments obtained in triplicate. An analysis of variance (ANOVA) was used to test the significance of the results using SPSS 19.0 software and $p < 0.05$ was considered to be statistically significant.

3. Results and discussion

3.1. Degradation of TCPP under different conditions in the PS+Fe^0+MC treatment process

The degradation of TCPP by the PS+Fe^0+MC process was studied and the efficiency of degradation of TCPP by this method was compared with degradation by Fe^0 + persulfate and a mechanochemical process + persulfate. Fig. 1 shows that the PS+Fe^0+MC process can degrade TCPP effectively. The material ratio (the mass of co-milling regent to the mass of the target pollutant) is one of the most important factors affecting the MC method (Liu et al., 2016b). Fig. 1a shows that the degradation efficiency of TCPP increased as the material ratio increased when the ratio of ZVI to persulfate was 4:1. When the material ratio reached 20:1 and 30:1, the degradation efficiencies of TCPP 1 and TCPP 2 were >90% after ball-milling for 2 h. When the material ratio was 30:1, the degradation efficiencies of TCPP 1 and TCPP 2 were as high as 97.10 and 98.17%, respectively. However, when the material ratio was 10:1, the degradation efficiencies of TCPP 1 and TCPP 2 were only 77.76 and 70.01%, respectively. These results show that as the material ratio increases, an increase in the ZVI and persulfate content increases the degradation efficiency of TCPP. ZVI provides electrons during the ball-milling process, which activate persulfate to generate free radicals, which, in turn, attack the chlorine atoms in pollutants and accelerate the process of dechlorination .

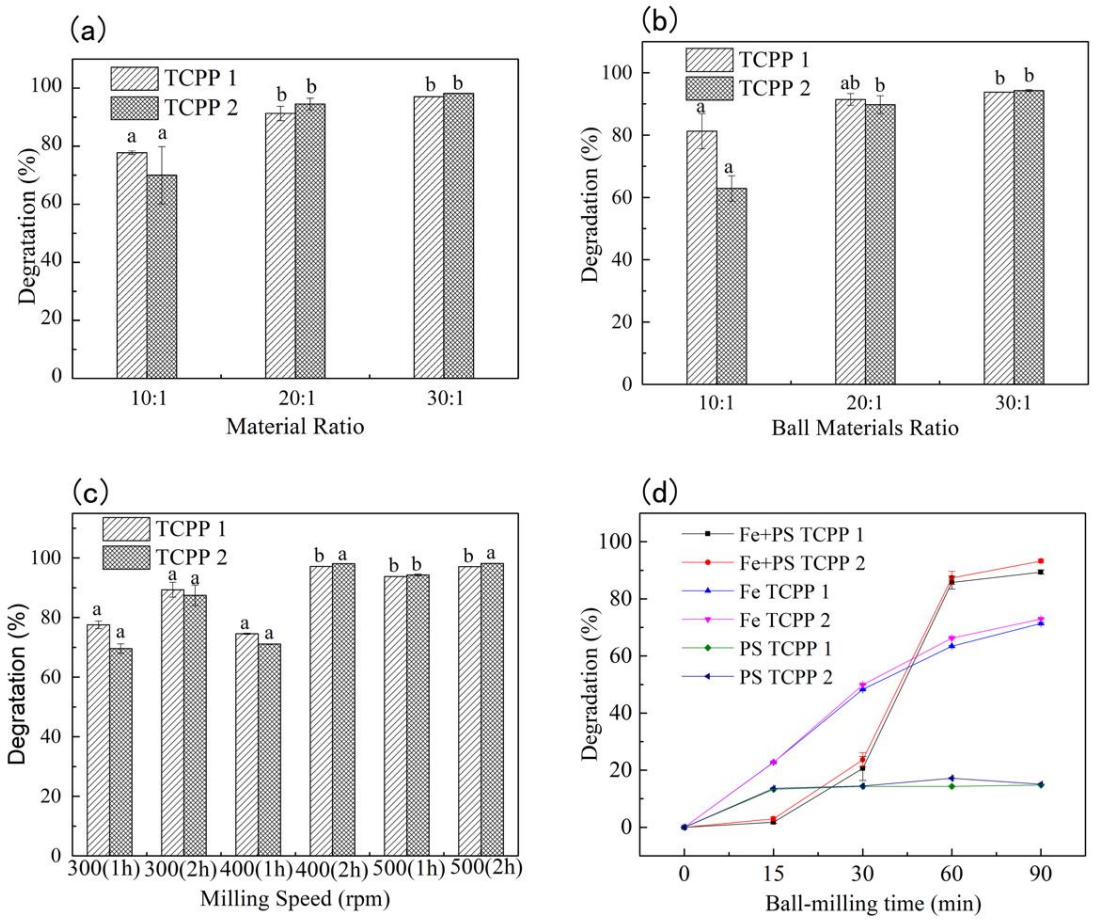

202

203 Fig. 1. Degradation efficiency of TCPP by the PS+Fe^0+MC process under different (a)

204 material ratios (ratio of ZVI and persulfate 4:1, with ball-milling for 2 h), (b) ball to

205 material ratios and (c) milling speeds. (d) Comparison with different co-milling

206 reagents. Different letters indicate a significant difference at $p < 0.05$

207

208 The BMR is another important factor affecting MC degradation. Three BMRs

209 (10:1, 20:1 and 30:1) were selected. Fig. 1b shows that the efficiencies of the MC

210 degradation of TCPP increased with an increase in the BMR. When the BMR was 30:1,

211 the degradation efficiencies of TCPP 1 and TCPP 2 were 93.78 and 94.30%,

212 respectively, but the degradation efficiencies of TCPP 1 and TCPP 2 were only 81.24

213 and 62.87% when the BMR was 10:1. This is because the collision energy increases as
214 the mass of the milling balls increases, which favors the degradation of pollutants . The
215 removal of pollutants is also related to the collision power. The collision power includes
216 the collision energy and the collision frequency (Abdellaoui & Gaffet, 1995). The
217 collision frequency in the ball mill tank increases as the number of milling balls
218 increases. However, too many milling balls reduce the space available for the
219 movement of balls in the ball-milling tank, which decreases both the collision speed
220 and energy (Sui et al., 2017).

221 Fig. 1c shows the effect of milling speed on the degradation of TCPP and indicates
222 that the degradation efficiency increases with an increase in the milling speed. The
223 degradation efficiencies of TCPP 1 and TCPP 2 reached 93.79 and 94.30%, respectively,
224 after 1 h of milling time at 500 rev min^{-1}. The kinetic energy in a planetary ball mill is
225 transferred during the ball-milling process and the speed determines the total energy
226 input from the ball mill (Abdellaoui & Gaffet, 1995). As the rotation speed increases,
227 the collision speed and frequency of the milling ball and the target pollutant increase,
228 which results in a high mechanical energy of the mixture in the tank, thereby converting
229 it into chemical energy. The MC reaction is therefore accelerated, resulting in the rapid
230 degradation of the pollutant . The removal efficiency of TCPP was >97% at 400 and
231 500 rev min^{-1} after 2 h of milling time.

232 Fig. 1d shows the degradation of 0.16 g TCPP with persulfate, ZVI or a mixture
233 of ZVI and persulfate as the co-milling regents (4.84 g). After milling for 2 h, the

degradation efficiencies of TCPP 1 were 20.21, 80.15 and 95.50% in the MC+persulfate (MC+PS), MC+Fe^0 and PS+Fe^0+MC experiments, respectively. The degradation efficiencies of TCPP 2 were 20.21, 75.93 and 96.50% in the MC+PS, MC+Fe^0 and PS+Fe^0+MC experiments, respectively. The degradation efficiency of TCPP did not change when persulfate alone was used as the co-milling reagent. The degradation efficiency increased with an increase in the milling time for the Fe^0+MC and the PS+Fe^0+MC systems. After 45 min of ball-milling, the PS+Fe^0+MC system had the highest degradation efficiency of TCPP.

A combination of ZVI and persulfate has been used previously as an advanced oxidation method to remove organic pollutants from water (Oh et al., 2009, Wei et al., 2016). As a strong oxidant, persulfate can be activated by ultraviolet light, heating or transition metals to generate sulfate radicals that can oxidize and decompose pollutants. Metals can produce lattice defects after ball-milling and then generate a large number of electrons, which favors electron transfer in the dechlorination process (Cagnetta et al., 2017). Therefore the Fe^{2+} produced by the electron transfer of ZVI can activate persulfate to generate $SO_4\cdot^-$ to promote the removal of TCPP.

The particle shape and size of the co-milling agents also can affect the efficiency of the degradation of pollutants. In this study, small particles were adsorbed onto the surface of large particles and large agglomerates formed, suggesting that the large particles would break and form a new surface after ball-milling (Fig. S3). The particle size of the co-milling agents decreased with increasing milling time (Fig. S4). After

255 milling for 60 min, the number of particles >45 μm decreased. After milling for 120
256 min, particles >45 μm disappeared completely, showing that the degradation of TCPP
257 continued over time (Wang et al., 2020). The smaller the particle size and the larger the
258 specific surface area of ZVI, the stronger the reaction activity. Small size was beneficial
259 for ZVI to stimulate PS to produce $SO_4^{\cdot -}$ and reduce organic pollutants

260 **3.2. Dechlorination and mineralization of TCPP**

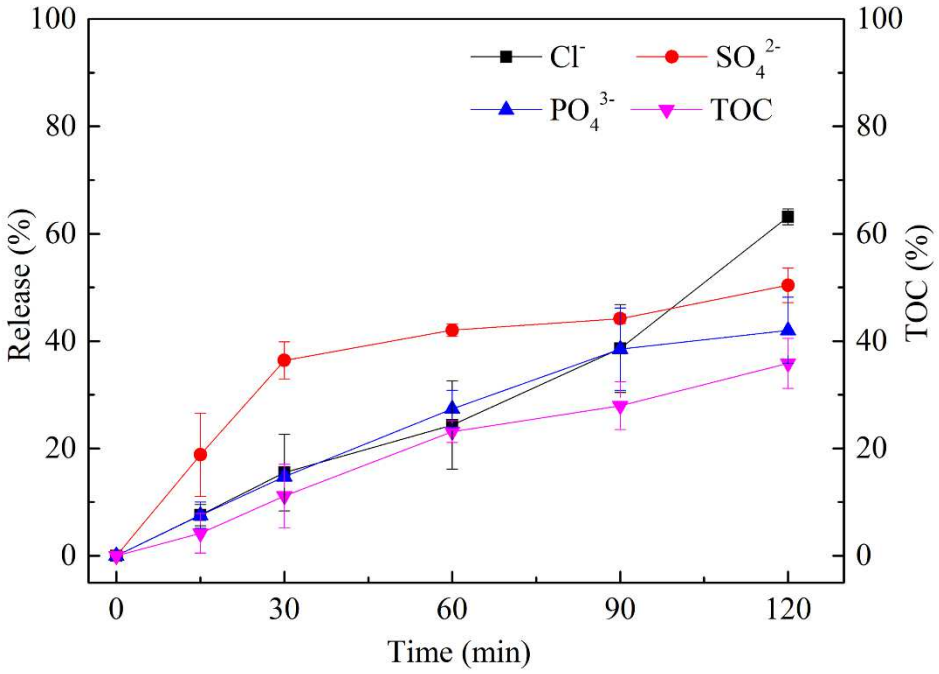

261

262 Fig. 2. Ion release rate and removal rate of total organic carbon from ball-milled
263 samples at different times

264

265 The molecular structure of TCPP contains a phosphoric acid center and three
266 chlorinated alkyl chains. When the free radicals generated during the ball-milling
267 process attack the TCPP molecule, Cl^- and PO_4^{3-} are released and $S_2O_8^{2-}$ is converted

to SO_4^{2-}. Fig. 2 shows that the release efficiencies of Cl^-, SO_4^{2-} and PO_4^{3-} increased as the ball-milling time increased. The release of SO_4^{2-} was higher than that of Cl^- and PO_4^{3-} until a milling time of 90 min. After ball-milling for 2 h, the release efficiencies of Cl^-, SO_4^{2-} and PO_4^{3-} were 63.16, 50.39 and 42.01%, respectively.

TCPP can be dechlorinated to phosphorus-containing organic species, the organic group of which is removed to produce PO_4^{3-}. In addition, PO_4^{3-} is not completely released, indicating that the phosphoric acid center of TCPP is difficult to destroy completely. When compared with the high degradation efficiency of TCPP, the dechlorination of TCPP is not complete, which indicates that a large number of chlorine-containing degradation intermediates are produced during the MC degradation of TCPP. Fig. 2 also shows that the removal efficiency of total organic carbon only reaches 35.87%, indicating that TCPP is not completely mineralized, consistent with the results of Liu et al. (2017).

3.3. Characterization of milled samples

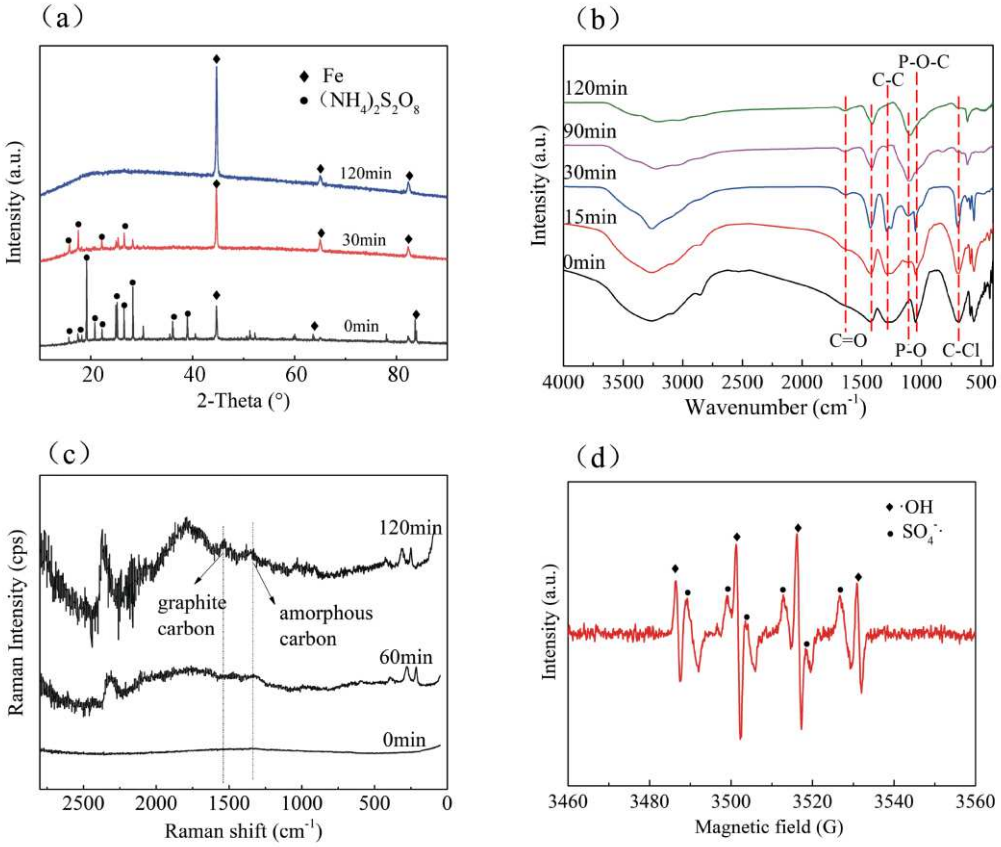

283

284 Fig. 3. (a) XRD, (b) FTIR, (c) Raman spectra of the ball-milled samples at different

285 times and (d) the electron spin resonance spectra of samples ball-milled for 0.5 h.

286

287 FTIR, XRD and Raman analyses were carried out on the ball-milled samples to

288 clarify the mechanism of MC degradation of TCPP. FTIR spectrometry was used to

289 determine the changes in the characteristic FTIR peaks of the functional groups in the

290 TCPP molecules during ball-milling (Table S1).

291 Fig. 3a shows the XRD spectra of the milled samples for different milling times.

292 After milling for 30 min, the characteristic peak for persulfate weakened, indicating

293 that the PS+Fe^0+MC process rapidly destroyed TCPP. After milling for 2 h, the Fe peak

294 was greatly increased and the persulfate peak completely disappeared, indicating that

295 the increased crystallinity of Fe activated persulfate, which has a major role in the
296 degradation of TCPP in the ball-milling process. In addition, the Fe peak was broadened
297 with the increasing milling time, indicating that the distortion of Fe lattice increased,
298 which provided more free electrons for the redox process in the degradation of TCPP
299 (Sui et al., 2017).

300 Fig. 3b shows that the C–Cl peak at 695 cm^{-1} decreased with an increase in the
301 ball-milling time, indicating that the Cl atom in TCPP was gradually removed to form
302 Cl^- . The peaks at 1049, 1281 and 1428 cm^{-1}, which represent the P–O–C and C–C
303 bonds and the CH_2 group, respectively, decreased with an increase in the milling time
304 (Yan et al., 2017, Zhang et al., 2020), which shows that the chloropropane group linked
305 to the ether bond was removed from TCPP. The fracture of the C–C bond means that
306 the chloropropane side-chain was broken down to form smaller molecules. The peaks
307 at about 1100 cm^{-1}, characteristic of the P–O bond, increased after ball-milling (Siow
308 et al., 2014), which indicates that the number of phosphoric acid groups increased. The
309 peak at 1642 cm^{-1} related to the C=O bond appeared during ball-milling, which means
310 that carbonyl groups formed in the product.

311 As the milling time increased, the color of the MC degradation product deepened
312 and the product turned completely black after milling for 2 h (Fig. S5), suggesting that
313 the samples were carbonized, which was confirmed by the Raman spectra (Fig. 3c).
314 The peak of the initial TCPP was unclear after 1 h of ball-milling. After milling for 2 h,
315 two peaks at appeared at the D-band (1330~1380 cm^{-1}) and the G-band (1540~1580

316 cm^{-1}), which correspond to the typical Raman spectra of amorphous carbon and
317 graphite, respectively (Wakayama et al., 1999). The appearance of the D and G peaks
318 in the Raman spectra suggests that TCPP was carbonized to carbon materials with
319 defective and disordered structures (Xu et al., 2013). The sequence of peaks D and G
320 showed that the carbonization process first generated amorphous carbon and then part
321 of the carbon product was converted to graphite. Zhang et al. (2011) reported that
322 pentachloronitrobenzene can be converted to amorphous carbon and graphite during
323 milling with Fe. The intensity of the D and G peaks was not high, which showed that
324 only part of the TCPP was mineralized through carbonization. This shows that it is
325 difficult to fully mineralized TCPP and that mineralization was not the only pathway
326 used to degrade TCPP.

327 ESR was used to identify the active species in the PS+Fe^0+MC system for selected
328 samples ball-milled for 30 min. Fig. 3d shows that the characteristic peaks of ·OH and
329 SO_4·$^-$ appeared, indicating that ·OH and SO_4·$^-$ were produced during the ball-milling
330 process(Yin et al., 2020). This result confirmed that the degradation of TCPP by the
331 MC process was a result of oxidation by ·OH and SO_4·$^-$.

3.4. Mechanism of activation of persulfate

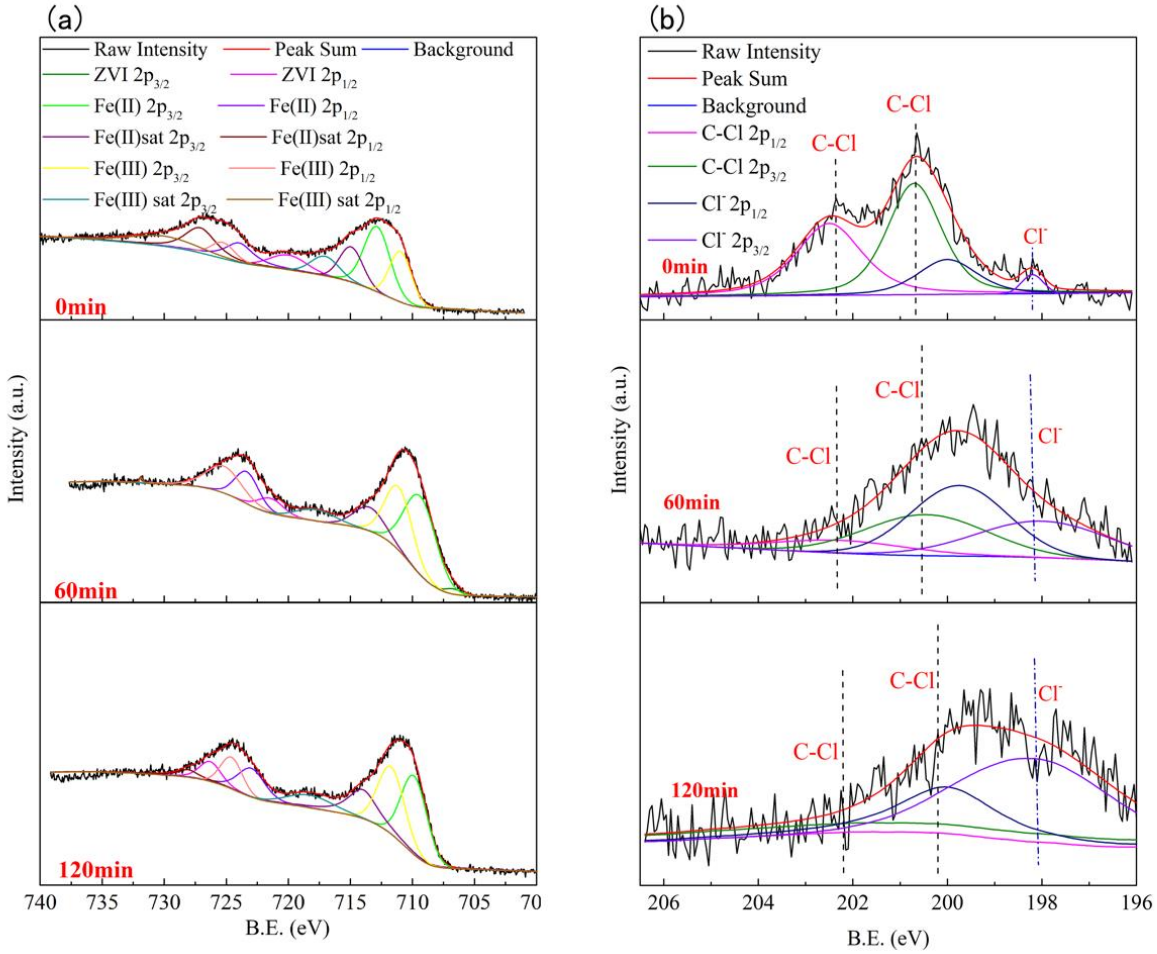

Fig. 4. XPS spectra of (a) Fe 2p and (b) Cl 2p of ball-milled samples at different times

XPS was used to analyze the chemical composition and changes in the valence of the elements on the surface of the sample to investigate the degradation mechanism of TCPP. All the XPS peaks were calibrated using the C1s peak at 284.8 eV. Table S2 gives the specific binding energy positions of the fitted peaks of ZVI in the initial sample (Deng et al., 2020). The changes in the peak areas of samples Fe^0, Fe^{2+} and Fe^{3+} at different milling times were compared.

Fig. 4a shows that the peak area of ZVI decreased with an increase in the milling

time, whereas the peak areas of Fe^{2+} and Fe^{3+} increased. This suggests that ZVI was oxidized to Fe^{2+} by persulfate during the ball-milling process with the formation of SO_4^{2-} (Eq. (1)) (Al-Shamsi & Thomson, 2013). Some of the Fe^{2+} was oxidized further to Fe^{3+}. The persulfate ($S_2O_8^{2-}$) was converted into SO_4^{2-} and $SO_4\cdot^-$ (Eq. (2)) (Oh et al., 2009). Some of the Fe^{2+} reacted with the sulfate radicals generated in Eq. (2) to produce Fe^{3+} and SO_4^{2-} (Eq. (3)) (Kishi & Ikeda, 1973). However, as shown in Fig. S6, the concentration of the produced Fe^{2+} was far higher than that of Fe^{3+}, showing Fe^{3+} is easy to be reduced to Fe^{2+} in MC process (Eq.(5)). The results shows that the degradation of TCPP by the PS+Fe^0+MC process was accompanied by the generation of SO_4^{2-}, consistent with the increase in the release rate of SO_4^{2-} shown in Fig. 2 (Deng et al., 2020). The SO_4^- generated in Eq. (2) reacted with water (present in humid air and in additives) to generate hydroxyl radicals (·OH) and $SO_4\cdot^-$ (Eq. (4)). These results all confirm that persulfate can be activated by ZVI to generate $SO_4\cdot^-$ and ·OH radicals, thereby promoting the degradation of TCPP. Finally, the reduction reaction of ZVI could remove chlorine in the micromolecular chlorinated organics which were the intermediate products during the MC process (Eq. (6)).

$$Fe^0 + S_2O_8^{2-} \rightarrow Fe^{2+} + 2SO_4^{2-} \quad (1)$$

$$Fe^{2+} + S_2O_8^{2-} \rightarrow Fe^{3+} + SO_4\cdot^- + SO_4^{2-} \quad (2)$$

$$Fe^{2+} + SO_4\cdot^- \rightarrow Fe^{3+} + SO_4^{2-} \quad (3)$$

$$H_2O + SO_4\cdot^- \rightarrow \cdot OH + SO_4^{2-} + H^+ \quad (4)$$

$$Fe^{3+} + Fe^0 \rightarrow Fe^{2+} \quad (5)$$

364 $Fe^0 + R\text{-}Cl \rightarrow Fe^{2+} + Cl^- + RH$ (6)

365

366 Fig. 4b shows the change in valency of chlorine. In the initial stage, the
367 characteristic peaks of the C–Cl bond appeared at about 200.7 and 202.5 eV and a weak
368 Cl^- peak was seen at about 198.2 eV (Moulder et al., 1992). After ball-milling for 1 h,
369 the characteristic peak of the C–Cl bond gradually weakened until it disappeared at 2 h,
370 whereas the characteristic peak of Cl^- gradually strengthened. This shows that TCPP
371 was destroyed and the organic chlorine in the TCPP molecule was transformed into
372 inorganic chlorine.

373

374 **3.5. Degradation pathways of TCPP in PS+Fe^0+MC treatment**

375 The degradation products of TCPP1 were analyzed by LC–QTOF-MS and five
376 intermediate products were detected: $C_6H_{13}Cl_2O_4P$ (product A, *m*/*z* 251.0); $C_3H_8ClO_4P$
377 (product B, *m*/*z* 175.0); $C_9H_{17}Cl_2O_5P$ (product C, *m*/*z* 307.0); $C_9H_{17}Cl_2O_6P$ (product D,
378 *m*/*z* 323.0) and $C_6H_{12}Cl_2O_6P$ (product E, *m*/*z* 247.0). Table S7 shows the corresponding
379 information and mass spectra.

380 Two degradation pathways of TCPP are proposed (Fig. 5). The first pathway is the
381 P–O–C cleavage pathway, which is similar to the oxidative degradation of organic
382 phosphorus compounds (Cheng et al., 2020). The ·OH generated by the activation of
383 persulfate attacks the phosphate center of TCPP and TCPP is cleaved at the P–O–C
384 bond to form the hydroxylated product A and 1-chloropropane . Product A is oxidized

by the same process to form product B, producing a third 1-chloropropane and PO_4^{3-}.

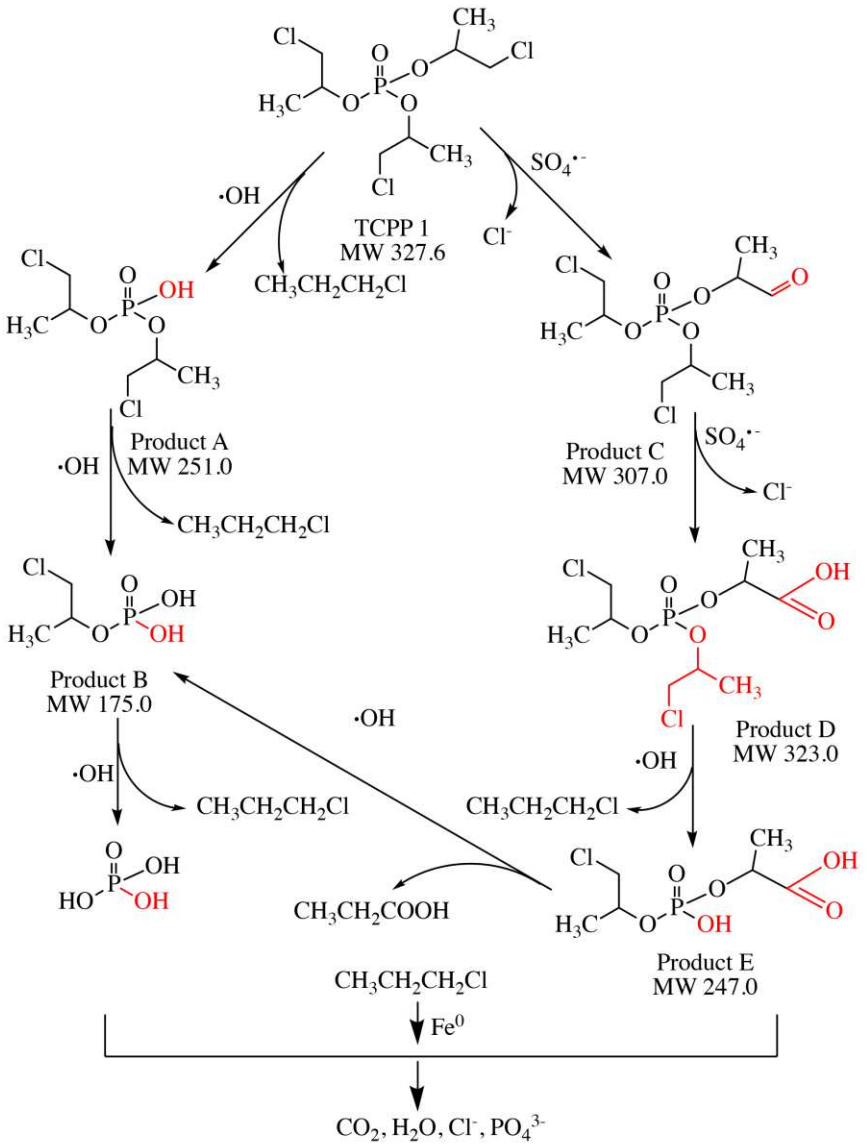

Fig. 5. Proposed degradation pathways of TCPP

In the second pathway, the C–Cl at the end of the alkyl chain of TCPP is oxidized by $SO_4^{\cdot-}$ to form a carbonyl compound (product C), which, in turn, is oxidized to produce a carboxylic acid (product D). The C–Cl bond in product D cannot be oxidized further, but the phosphate center in product D is attacked by the same route as the first

pathway. Product D is removed from one of the 1-chloropropane molecules to form product E, the P–O–C bonds of which are broken, followed by the formation of propionic acid through substitution, addition and $SO_4\cdot^-$ cleavage (Yu et al., 2019). The oxidative dechlorination in the second pathway confirms that the role of ZVI is not to reduce TCPP, but to activate persulfate to oxidize TCPP in the PS+Fe^0+MC system (Li et al., 2021).

The degradation mechanism includes oxidation, dechlorination, hydroxylation and dealkylation. ·OH and $SO_4\cdot^-$ mainly attack the phosphate center and the C–Cl bond at the end of the alkyl chain through substitution, addition and a series of electron transfer reactions. TCPP was converted into Cl^-, PO_4^{3-} and some intermediate products. However, $SO_4\cdot^-$ could not oxidize C-Cl bond in micromolecular organochlorides, while ZVI activated by MC could play the role in reductive dichlorination.

3.6 Toxities of TCPP and its MC degradation intermediates

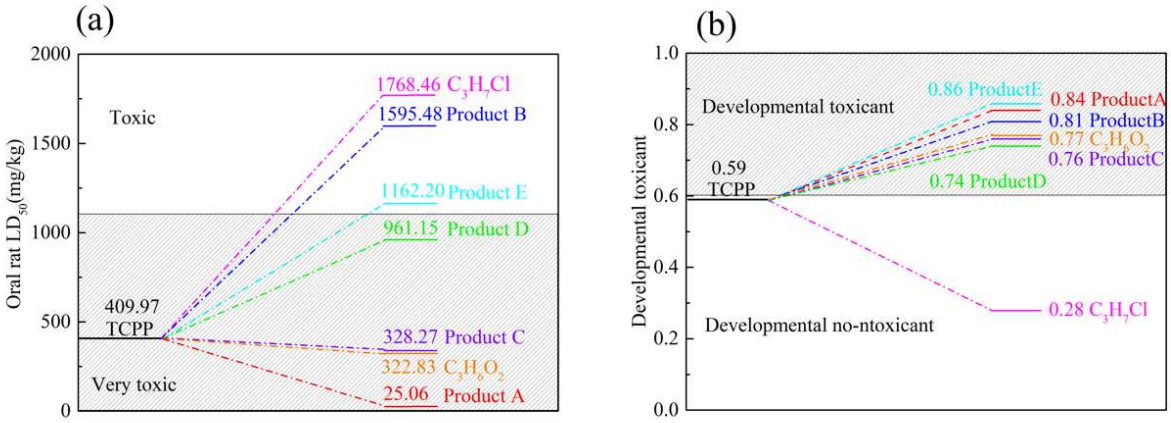

Fig. 6 Toxicities of TCPP and its MC degradation intermediates

Environmental Protection Agency toxicity estimation software tool (TEST) version 5.1 was used to evaluate the toxicity of TCPP and its degradation intermediates. In the TEST software, the 50% lethal dose (LD_{50}) of oral rats was selected as an index to predict the acute toxicities of the degraded intermediate products. As shown in Fig.6 (a), the LD_{50} of TCPP was 409.97mg/kg, which is considered "very toxic". After ball milling, the LD_{50} values of some intermediates were converted into "toxic" areas, while others still maintained in the "very toxic" areas. The results shows that PS+Fe^0+MC process reduced the toxicity of LD_{50}, and TCPP can be converted into some low-toxic products.. However, most of intermediates showed developmental toxicant more than that of TCPP (Fig. 6b). Although TCPP could be almost completely degraded via PS+Fe^0+MC process, the toxicity of the intermediates did not effectively removed because TCPP could not be completely mineralized by MC. So, the risk resulted from MC degradation of TCPP cannot be ignored.

3.7 Degradation of TCPP in soils by MC with ZVI and PS

As shown in Fig. 7, after milling for 2 h, the degradation rates of TCPP 1 in red soil, yellow soil and black soil were 92.13%, 85.76% and 83.83%, respectively, and the degradation rates of TCPP 2 were 90.80%, 87.38% and 87.01%, respectively. To clarify the relation between the degradation rates of TCPP and characteristics of soils, the pH, iron contents and organic matter contents of three soils were detected (Table S2). The results showed that the degradation of TCPP was high under acid conditions. The

previous studies have shown that PS is easily activated to generate $SO_4^{\cdot-}$ and ·OH under low pH conditions, and increasing pH inhibited the formation of $SO_4^{\cdot-}$ and ·OH . Iron concentration is another important influencing factor (Fan et al., 2018). The degradation of TCPP in red soil was faster than that of the other types of soils because iron concentration in red soil was higher than that of other two soils. The higher the iron concentration in soil, the higher the degradation of TCPP. This is because the presence of iron can promote the production of $SO_4^{\cdot-}$ from PS to degrade pollutants rapidly.

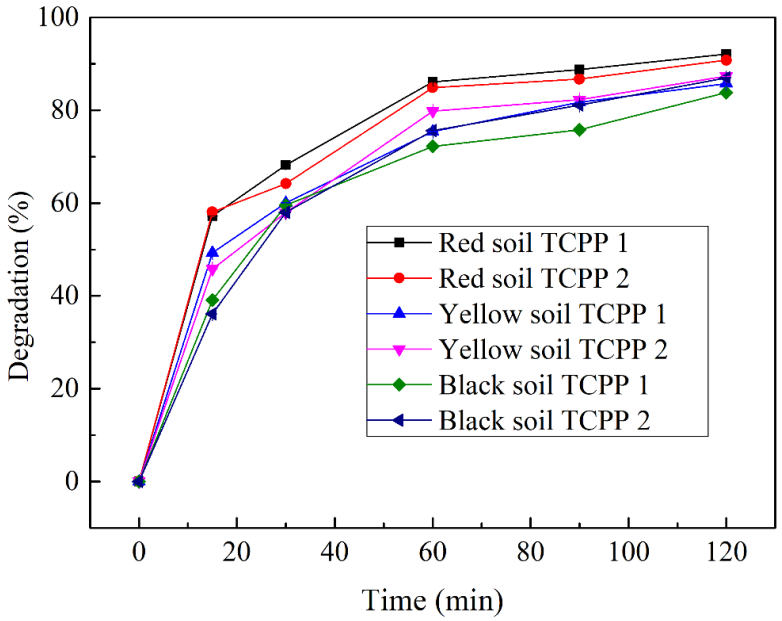

Fig. 7. Effect of soil types on TCPP degradation. The concentration of TCPP: 200mg/kg; mass ratio of soil to PMS: 18:1; BMR: 30:1; rotation speed: 400 rpm

In addition, the order of organic matter contents in different soils were: red soil < yellow soil < black soil. After ball milling for 2 h, the degradation rates of TCPP in the soil were: red soil > yellow soil > black soil. The results showed that the content of

445 organic matter in soils affected negatively the degradation rates, which confirmed the
446 previous research (Fan et al., 2018). In addition, during the first 15min of MC
447 degradation, the removal efficiencies of TCPP in soil were higher than that of TCPP
448 without soil mixture, which was because that metal oxide in soil might promote the
449 degradation rates of MC to TCPP. Therefore, we suppose that PS+Fe^0+MC process is a
450 promising method for the removal of organic pollutants in soil.
451

452 ## 4. Conclusions

453 This study shows that the PS+Fe^0+MC process is an effective method for the
454 degradation of TCPP. The degradation efficiency was as high as 96.5% after milling for
455 2 h with a material ratio of 30:1, a BMR of 30:1 and a milling speed of 400 rev min^{-1}.
456 The ·OH formed in the combination process attacked the P–O–C bonds in phosphate
457 center of TCPP, meanwhile a C–Cl bond in part of the TCPP molecule was oxidized by
458 SO_4·$^-$ to carbonyl and carboxyl groups. resulting in dechlorination via oxidation of the
459 C–Cl bond. Finally, ZVI reductively dechlorinated the intermediate organochloride
460 products, resulting in the mineralization of TCPP due to the synergistic effect of the
461 reduction of ZVI and the oxidation reaction of ·OH and SO_4·$^-$ in MC process although
462 LD_{50} and developmental toxicant of the intermediate products were not completely
463 removed. These results show that persulfate can be used in the MC degradation of
464 organic pollutants; moreover, pollutants in soils can be degraded via the MC methods.
465 The PS+Fe^0+MC system is an efficient and environmentally friendly method that is

widely used to remove organic phosphorus pollutants.

Author contribution W. Qiao and Q. Yang designed the work, performed MC degradation and sampling, and performed all parameters' measurements used in this project. Y. Qian and Z. Zhang analyzed data and participates in the interpretation of data. W. Qiao and Q. Yang contributed to drafting and critically revising of the paper. All authors gave final approval of the version to be published, and agreed to be accountable for all aspects of the work.

Funding This work was financially supported by the Natural Science Foundation of Jiangsu Province (BK20201388), the Industry Prospect and Common Key Technologies in Jiangsu Province (BE2018015) and the Priority Academic Program Development of Jiangsu Higher Education Institutions (PAPD).

Availability of data and materials The datasets used or analyzed during the current study are available from the corresponding author on reasonable request.

Declarations

Ethics approval Not applicable.

Consent to participate Not applicable.

Consent to Publish Not applicable.

Competing interests The authors declare no competing interests

References

Abdellaoui M, Gaffet E (1995) The physics of mechanical alloying in a planetary ball mill: Mathematical treatment. Acta Metallurgica et Materialia 43: 339-344

Al-Shamsi MA, Thomson NR (2013) Treatment of organic compounds by activated persulfate using nanoscale zerovalent iron. Industrial Engineering Chemistry Research 52: 13564-13571

Björklund J, Isetun S, Nilsson U (2004) Selective determination of organophosphate flame retardants and plasticizers in indoor air by gas chromatography, positive-ion chemical ionization and collision-induced dissociation mass spectrometry. Department of Analytical Chemistry, Stockholm University, S-106 91 Stockholm, Sweden. 18: 3079-3083

Cagnetta G, Huang J, Lu M, Wang B, Wang Y, Deng S, Yu G (2017) Defect engineered oxides for enhanced mechanochemical destruction of halogenated organic pollutants. Chemosphere 184: 879-883

Cagnetta G, Robertson J, Huang J, Zhang K, Yu G (2016) Mechanochemical destruction of halogenated organic pollutants: a critical review. J Hazard Mater 313: 85-102

Cheng Z, Chen Q, Cervantes S, Tang Q, Gao X, Tan Y, Liu S, Ma Y, Shen Z (2020) Two-dimensional and three-dimensional quantitative structure-activity

relationship models for the degradation of organophosphate flame retardants during supercritical water oxidation. J Hazard Mater 394

Deng S, Bao Y, Cagnetta G, Huang J, Yu G (2020) Mechanochemical degradation of perfluorohexane sulfonate: Synergistic effect of ferrate(VI) and zero-valent iron. Environmental Pollution 264: 114789

Dong Y, Li Y, Zhao C, Feng Y, Dong Y (2019) Mechanism of the rapid mechanochemical degradation of hexachlorobenzene with silicon carbide as an additive. J Hazard Mater 379: 120653

Dubinskaya AM (2010) Transformations of organic compounds under the action of mechanical stress. Russian Chemical Reviews 68: 637-652

Fan G, Liu X, Li X, Lin C, He M, Ouyang W (2020) Mechanochemical treatment with CaO-activated PDS of HCB contaminated soils. Chemosphere 257

Fan G, Liu X, Lin C, Li PJEC (2018) Peroxymonosulfate assisted mechanochemical method for the degradation of phenanthrene in contaminated soils. Emerging Contaminants 4: 22-31

Hoffman K, Daniels JL, Stapleton HM (2014) Urinary metabolites of organophosphate flame retardants and their variability in pregnant women. Environ Int 63: 169-172

Jurgens SS, Helmus R, Waaijers SL, Uittenbogaard D, Dunnebier D, Vleugel M, Kraak MHS, De Voogt P, Parsons JR (2014) Mineralisation and primary biodegradation of aromatic organophosphorus flame retardants in activated sludge. Chemosphere 111: 238-242

529 Kishi K, Ikeda S (1973) X-Ray photoelectron spectroscopic study for the reaction of
530 evaporated iron with O and H2O. Bull Chem Soc Jpn 46: 341-345
531 Li D, Zhong Y, Zhu X, Wang H, Yang W, Deng Y, Huang W, Peng Pa (2021) Reductive
532 degradation of chlorinated organophosphate esters by nanoscale zerovalent
533 iron/cetyltrimethylammonium bromide composites: Reactivity, mechanism and
534 new pathways. Water Res 188
535 Liu J, Li C, Zhou P, Wu S, Ou H (2017) Heterogeneous photocatalysis of tris(2-
536 chloroethyl) phosphate by UV/TiO_2: Degradation products and impacts on
537 bacterial proteome. Water Res 124: 29-38
538 Liu X, Zhang X, Shao K, Lin C (2016a) Fe0-activated persulfate-assisted
539 mechanochemical destruction of expired compound sulfamethoxazole tablets. Rsc
540 Advances 6: 20938-20948
541 Liu X, Zhang X, Zhang K, Qi C (2016b) Sodium persulfate-assisted mechanochemical
542 degradation of tetrabromobisphenol A: efficacy, products and pathway.
543 Chemosphere 150: 551-558
544 Moulder JF, Chastain J, King RC (1992) Handbook of x-ray photoelectron
545 spectroscopy : a reference book of standard spectra for identification and
546 interpretation of XPS data. Chem Phys Lett 220: 7-10
547 Oh SY, Kim HW, Park JM, Park HS, Yoon C (2009) Oxidation of polyvinyl alcohol by
548 persulfate activated with heat, Fe^{2+}, and zero-valent iron. J Hazard Mater 168: 346-
549 351

Quintana JB, Rodil R, Reemtsma T, García-López M, Rodríguez I (2008) Organophosphorus flame retardants and plasticizers in water and air II. Analytical methodology. TrAC, Trends Anal Chem 27: 904-915

Ruan XC, Ai R, Jin X, Zeng QF, Yang ZY (2013) Photodegradation of tri (2-chloroethyl) phosphate in aqueous solution by UV/H_2O_2. Water, Air, Soil Pollut 224: 1-10

Siow KS, Britcher L, Kumar S, Griesser HJ, Polymers (2014) Deposition and XPS and FTIR analysis of plasma polymer coatings containing phosphorus. Plasma Processes and Polymers 11: 133-141

Sui H, Rong Y, Song J, Zhang D, Li H, Wu P, Shen Y, Huang Y (2017) Mechanochemical destruction of DDTs with Fe-Zn bimetal in a high-energy planetary ball mill. J Hazard Mater 342: 201-209

Un-Jung, Kim, Jung, Keun, Oh, Kurunthachalam, Kannan (2017) Occurrence, removal, and environmental emission of organophosphate flame retardants/plasticizers in a wastewater treatment plant in New York state. Environ Sci Technol 14: 7872-7880

Veen IVD, Boer JD (2012) Phosphorus flame retardants: Properties, production, environmental occurrence, toxicity and analysis. Chemosphere 88: 1119-1153

Wakayama H, Mizuno J, Fukushima Y, Nagano K, Fukunaga T, Mizutani UJC (1999) Structural defects in mechanically ground graphite. Carbon 37: 947-952

Wang G, Chen H, Du Z, Li J, Wang Z (2017) In vivo metabolism of organophosphate flame retardants and distribution of their main metabolites in adult zebrafish. Sci Total Environ 590-591: 50-59

571 Wang N, Lv H, Zhou Y, Zhu L, Tang H (2019) Complete defluorination and
572 mineralization of perfluorooctanoic acid by a mechanochemical method using
573 alumina and persulfate. Environ Sci Technol 53: 8302-8313
574 Wang R, Zhu Z, Tan S, Guo J, Xu Z (2020) Mechanochemical degradation of
575 brominated flame retardants in waste printed circuit boards by ball milling. J
576 Hazard Mater 385: 121509
577 Wei X, Gao N, Li C, Yang D, Zhou S, Lei L (2016) Zero-valent iron (ZVI) activation
578 of persulfate (PS) for oxidation of bentazon in water. Chem Eng J 285: 660-670
579 Xu W, Mao N, Zhang J (2013) Graphene: a platform for surface‐enhanced raman
580 spectroscopy. Small 9: 1206-1224
581 Yan X, Liu X, Qi C, Lin C, Li P, Wang H (2017) Disposal of hexabromocyclododecane
582 (HBCD) by grinding assisted with sodium persulfate. Rsc Advances 7: 23313-
583 23318
584 Yan X, Liu X, Qi C, Wang D, Lin C (2015) Mechanochemical destruction of a
585 chlorinated polyfluorinated ether sulfonate (F-53B, a PFOS alternative) assisted
586 by sodium persulfate. Rsc Advances 5: 85785-85790
587 Yin Z, Han M, Hu Z, Feng L, Liu Y, Du Z, Zhang L (2020) Peroxymonosulfate
588 enhancing visible light photocatalytic degradation of bezafibrate by Pd/g-C3N4
589 catalysts: the role of sulfate radicals and hydroxyl radicals. Chem Eng J 390:
590 124532
591 Yu X, Yin H, Peng H, Lu G, Dang Z (2019) Degradation mechanism, intermediates and

592 toxicology assessment of tris-(2-chloroisopropyl) phosphate using ultraviolet
593 activated hydrogen peroxide. Chemosphere 241: 124991
594 Zhang W, Huang J, Xu F, Deng S, Zhu W, Yu G (2011) Mechanochemical destruction
595 of pentachloronitrobenzene with reactive iron powder. J Hazard Mater 198: 275-
596 281
597 Zhang Y, Tao H, Li J, Yang X (2020) Achieving a high-performance P/C anode through
598 P-O-C bond for sodium ion batteries. Ionics 26: 3377-3385
599
600

Supplementary Files

This is a list of supplementary files associated with this preprint. Click to download.

- SupplementaryMaterialESPR0528.docx